Earth Planet. Sci. Lett. 631 (2024) 118634

Contents lists available at ScienceDirect

Earth and Planetary Science Letters

journal homepage: www.elsevier.com/locate/epsl

Garnet zoning patterns record multiple processes of chemical transfer during subduction

Freya R. George [a,b,*], Daniel R. Viete [b], Janaína Ávila [c,d], Gareth G.E. Seward [e], George L. Guice [b,f,g,h], Mark B. Allen [i], Michael J. Harrower [b,j]

[a] School of Earth Sciences, University of Bristol, Bristol, BS8 1RJ, UK
[b] Department of Earth & Planetary Sciences, Johns Hopkins University, Baltimore, MD 21218, USA
[c] School of Earth and Environmental Sciences, The University of Queensland, St Lucia QLD 4072, Australia
[d] Research School of Earth Sciences, The Australian National University, Canberra ACT 0200, Australia
[e] Department of Earth Science, University of California, Santa Barbara, CA 93106, USA
[f] Department of Mineral Sciences, Smithsonian National Museum of Natural History, Washington D.C., 20560, USA
[g] Department of Earth & Planetary Sciences, American Museum of Natural History, New York City, NY 10024, USA
[h] Department of Physics, Astronomy & Geosciences, Towson University, Towson, MD 21252, USA
[i] Department of Earth Sciences, Durham University, Durham, DH1 3LE, UK
[j] Department of Near Eastern Studies, Johns Hopkins University, Baltimore, MD 21218, USA

ARTICLE INFO

Keywords:
Oscillatory zoning
Garnet
Subduction fluids
Oxygen isotopes

ABSTRACT

Subduction is the principal mechanism by which volatiles are transferred from the Earth's surface to its interior. In garnets from eclogites and blueschists formed within the subduction setting, fine-scale, oscillatory elemental zoning is a common feature, sometimes considered to record open-system fluid exchange during prograde metamorphism. We present oxygen isotope data for garnets with such zoning from five exhumed subduction zone complexes. Short length scale fluctuations in elemental and oxygen isotope zoning (which are themselves spatially decoupled) cannot be linked to open-system fluid exchange during garnet crystallization in all samples; these data do not provide evidence for a genetic relationship between elemental oscillations and fluid fluxing. However, garnets from one setting do provide clear evidence for syn-growth ingress of elementally and isotopically buffering fluids, a process that operated simultaneously with the formation of elemental oscillations. Our findings indicate multiple mechanisms of chemical transfer operate at the grain–rock scale during subduction, and that some subduction zone rocks may experience only limited interaction with external prograde fluids. These results are consistent with a picture of highly heterogenous volatile transfer during subduction, and suggest that some proportion of the fluid inventory inherited at shallow depths may be transferred to sub-arc depths.

1. Introduction

During subduction, prograde dehydration of oceanic lithosphere liberates large volumes of fluids. Understanding the fate of these fluids—released to the mantle wedge, mobilized up the slab–wedge interface, or transferred to sub-arc depths—is critical given their influence over arc magmatism, earthquake source processes, mass transfer, and chemical cycling between Earth's surface and interior (e.g., Schmidt and Poli, 1998; Collido et al., 2018). In high pressure–low temperature (*HP–LT*; eclogite and blueschist facies) metabasic rocks from subduction settings, garnet-bearing assemblages are common. Since first documented in Franciscan blueschists (Dudley, 1969), oscillatory chemical zoning (short-wavelength interface-parallel peaks and troughs in elemental concentration) in *HP–LT* garnet has been widely recognized (e.g., García-Casco et al., 2002; Kabir and Takasu, 2010; Li et al., 2016; Tual et al., 2022). Though it is clear that not every garnet from *HP–LT* settings carries oscillatory elemental zoning patterns (e.g., see Rubatto and Angiboust, 2015), empirical evidence seems to suggest that most *HP–LT* settings contain rocks with these features. Even in cases where major element oscillations are seemingly absent (e.g., due to diffusional homogenization or lack of analytical resolution), trace element mapping reveals that oscillations are often preserved in rare earth elements

* Corresponding author.
E-mail address: freya.george@bristol.ac.uk (F.R. George).

https://doi.org/10.1016/j.epsl.2024.118634
Received 1 August 2023; Received in revised form 21 February 2024; Accepted 23 February 2024
Available online 2 March 2024

(REEs; e.g., Rubatto et al., 2020; George et al., 2021; Konrad-Schmolke et al., 2023). This includes garnet-bearing rocks from subduction zones that differ with respect to their bulk composition, relative *P–T* path of metamorphism, and age. Given the widespread occurrence of this chemical feature, it is likely to record some fundamental process (or processes) that operates at garnet-stable conditions in subduction zones.

Numerous origins have been proposed for the formation of oscillatory zoning in garnet from a wide range of tectonic settings, including equilibrium responses to *P–T* cycling (e.g., García-Casco et al., 2002), major and accessory mineral breakdown (e.g., Pyle and Spear, 1999; Konrad-Schmolke et al., 2008b), changes in growth rate (George et al., 2018), and dissolution and reprecipitation (e.g., Jedlicka et al., 2015; Viete et al., 2018). Owing to the demonstrable relationship between fluid infiltration and oscillatory elemental zoning in minerals from other fluid-rich geological settings—including andradite garnet from hydrothermal skarns and contact aureoles (e.g., Jamtveit et al., 1995, Stowell et al., 1996), pyroxenes in mineralized shear zones and metasediments (Yardley et al., 1991; Schumacher et al., 1999), and in fluid-altered rinds of mélange rocks (Hoover et al., 2022)—similar zoning in *HP–LT* garnet is often attributed to grain boundary infiltration of external fluid that is out of equilibrium with garnet during its growth (e.g., Hickmott et al., 1992, Angiboust et al., 2014). Indeed, deformation-induced conduits and veins may facilitate long range transfer of chemically buffering subduction-related fluid, and minerals in these systems often have oscillatory elemental zoning (e.g., Spandler et al., 2011; Hoover et al., 2022; Angiboust and Raimondo, 2022).

In contrast to regions of macroscopic channelization, mechanisms responsible for grain-scale fluid and element transfer in nominally impermeable eclogites and blueschists remain poorly understood. Previous hypotheses include: (1) flow within an interconnected porosity driven by small- to large-scale gradients in stresses (e.g., Connolly and Poladchikov, 2004; Bovay et al., 2021); or (2) channelized transfer through, for example, veins produced by dehydration embrittlement (Camacho et al., 2005; John et al., 2012; Taetz et al., 2018), a reactive porosity (Plümper et al., 2017) or compaction channels (Piccoli et al., 2021).

Assessment of fluid (transfer) histories from crystal growth zoning has been made possible by increased analytical capabilities of stable isotope approaches (e.g., Baumgartner and Valley, 2001; Taetz et al., 2018; Gerrits et al., 2019; Penniston-Dorland et al., 2020). In particular, in situ measurement of the oxygen isotope composition ($\delta^{18}O$) of metamorphic minerals enables constraints to be placed on the sources and pathways of reactive fluids present during mineral re-crystallization. Slow oxygen diffusivities (e.g., Vielzeuf et al., 2005; Higashino et al., 2019; Scicchitano et al., 2021) ensure that $\delta^{18}O$ variations at scales of $<$10–100 μm in garnet are rarely modified by diffusion at *HP–LT* conditions, offering a record of prograde processes in eclogites and blueschists that cannot be accessed with the elemental record alone (e.g., Russell et al., 2013; Page et al., 2014; Cruz-Uribe et al., 2021; Bovay et al., 2021). Long wavelength core-to-rim $\delta^{18}O$ variation in garnet from metasomatized *HP–LT* rocks has been associated with influx of external fluids with distinct isotopic signatures, with positive shifts (2.5–4 ‰) attributed to channelized influx of isotopically-heavy, sediment-derived fluid (e.g., Russell et al., 2013; Rubatto and Angiboust, 2015; Page et al., 2019). Shifts to lower $\delta^{18}O$ values (by $\leq$8 ‰) have been attributed to infiltration of isotopically-light, serpentinite- or altered gabbro-derived fluids on either the prograde (e.g., Errico et al., 2013; Martin et al., 2014; Bovay et al., 2021) or retrograde path (Page et al., 2014; Cruz-Uribe et al., 2021). Oxygen isotope zonation has been documented in garnets displaying oscillatory elemental zoning (Bovay et al., 2021; Cruz-Uribe et al., 2021), in addition to garnets showing smooth prograde elemental zoning (e.g., Russell et al., 2013) or patchy metasomatic zoning (e.g., Errico et al., 2013; Rubatto and Angiboust, 2015).

Here, we utilize in situ measurements of major and trace elements and oxygen isotopes at the scale of individual growth zones to test the hypothesis that oscillatory zoning is demonstrably linked to repeated episodes of fluid infiltration and metasomatism in intact *HP–LT* rocks. Our results do not provide evidence for a genetic relationship between repeated external fluid infiltration and elemental oscillation formation. However, observed isotopic variation in garnet across multiple wavelengths does shed light on two end-member mechanisms of grain boundary fluid transfer during *HP–LT* garnet crystallization: (1) local, closed system chemical transfer resulting in muted, short-lengthscale isotopic variations; and (2) influx of externally-derived fluids that buffer the isotopic and elemental composition of garnet (see Errico et al., 2013; Rubatto and Angiboust, 2015; Bovay et al., 2021). The short-lengthscale isotopic patterns within and between garnet grains may be explained by temporally-variable grain boundary porosity and permeability within these overall closed systems, which maintains an isotopic heterogeneity with a maximum range of 1–2 ‰ across the centimeter-scale.

2. Methodology

The sample set is composed of *HP-LT* metabasites from five different subduction zones, including: amphibolite–eclogite from As Sifah (Oman; OM18–03) and Puerto Cabello (Venezuela; VE13–11), interlayered blueschist–eclogite from the Cycladic Blueschist Unit, Syros (Greece; SY15–10) and the Franciscan Complex, California (USA; CA13–01), in addition to core and rind samples from a lawsonite eclogite block of the Samana Complex, Punta Balandra (Dominican Republic; SS85–27E and SS85–27BC, respectively). Each site is a block-in mélange settings and has been well studied, providing good constraints on conditions of peak metamorphism and relative *P–T* paths during subduction.

However, unlike in previous studies that target macro-scale evidence of metasomatism in these settings (e.g., Rubatto and Angiboust, 2015; Hoover et al., 2022), samples that represent the dominant rock type of mélange blocks were mostly obtained from intact outcrop and were collected away from obvious fluid focusing structures. In each case, the *HP* metamorphic matrix assemblage has been modified by post-peak mineral growth. Specific samples for study were chosen based on electron probe microanalyzer (EPMA) X-ray maps that confirm the presence of oscillatory zoning in garnet. Constraints on *P–T*–time (*t*) conditions of metamorphism and photomicrographs of each are provided in Table 1 and Fig. 1, with full details in Supplementary Material (SM) 1.

Across rims of several garnets from each chosen sample, co-located transects for major elements and oxygen isotopes were acquired using EPMA at the University of California, Santa Barbara (USA) and the University of Ottawa (Canada), and secondary ionized mass spectrometry (SIMS) on the Sensitive High Resolution Ion Microprobe–Stable Isotope (SHRIMP–SI) at the Australian National University. Laser ablation–inductively coupled plasma–mass spectrometry (LA–ICP–MS) mapping was conducted on garnet from Oman at Johns Hopkins University (USA). Full details of the analytical methods are provided in SM 2.

3. Results

3.1. Major and trace element zoning in garnet

Multiple representative EPMA X-ray Mn maps from each *HP–LT* setting are presented in Fig. 2, and background corrected maps of Mg, Fe, Ca, Mn, and Al content for all 16 mapped garnets are presented in SM 3. All garnets display grain-scale core-to-rim decreases in Mn content and increases in Mg content. In mantle to rim regions, porphyroblasts contain concentric oscillatory major element zoning that is most pronounced in Mn and sometimes evident in Mg. Though the general form of the oscillations—interface-parallel peaks and troughs with a resolvable wavelength of 20–100 μm and an amplitude of 0.25–1.5 mol.% spessartine—is the same for all settings, their magnitude, positioning, and number varies between settings. The Ca and Fe maps (the two most

Table 1
Summary of samples used in this study. Mineral abbreviations after Whitney and Evans (2010). Additional detail and references provided in Supplementary Material 1.

Locality	Coordinates	Sample reference	Nature of sample	HP (+ retrograde) assemblage	Garnet diameter (mm); morphology	Peak T (°C)	Peak P (GPa)	Approx. age of (peak) metamorphism
Oman	23.43942°N, 058.76980°E	OM18-03B OM18-03C	Layers/pods in metased. mélange	Grt, Omp, Gln, Ph, Rt, Qz (Act, Ab, Chl, Cal, Py)	1–2, subhedral to anhedral	450–520	1.8–2.0	81–77 Ma[a]
Venezuela	10.46530°N, 067.94255°W	VE13-11	Block interior in metased. mélange	Grt, Omp, Amp, Zo, Rt, Qz (Ab, Amp, Chl)	<1; partially resorbed subhedral	(A) 550–600 (B) 450–520	(A) 1.6–1.8 (B) 1.8	28–42 Ma[b]
Greece	37.50175°N, 024.92664°E	SY15-10	Block interior in meta-volcanic melange	Grt, Gln, Omp, Ph, Alb, Rt, Zo, Lws (Chl, Ttn, Amph)	0.5–1; partially resorbed	480–550	1.4–1.8	52–50 Ma[c]
California	37.91788°N, 122.49305°W	CA13-01	Block interior in serp. mélange	Grt, Omp, Gln, Zo, Qz, Rt (Chl, Ttn)	<1; euhedral	555–585	1.4–1.95	157–158 Ma[d]
Dominican Republic	19.18206°N, 069.23367°W	SS85-27E	Eclogite block rind	Grt, Omp, Ph, Gln, Ep, Rt, Ttn, Qz (Chl, Hem)	<0.6–1; subhedral	(A) 450 ± 70 (B) 550–625	(A) 1.3 ± 0.2 (B) 2–2.4	115–110 Ma[e]
	19.18206°N, 069.23367°W	SS85-27BC1	Eclogite block core	Grt, Omp, Ph, Gln (Act, Ab, Chl)	1–3; euhedral			

[a] Garber et al., 2021.
[b] Viete et al., 2015.
[c] Lagos et al., 2007.
[d] Anczkiewicz et al., 2004.
[e] Blanco-Quintero et al., 2010b.

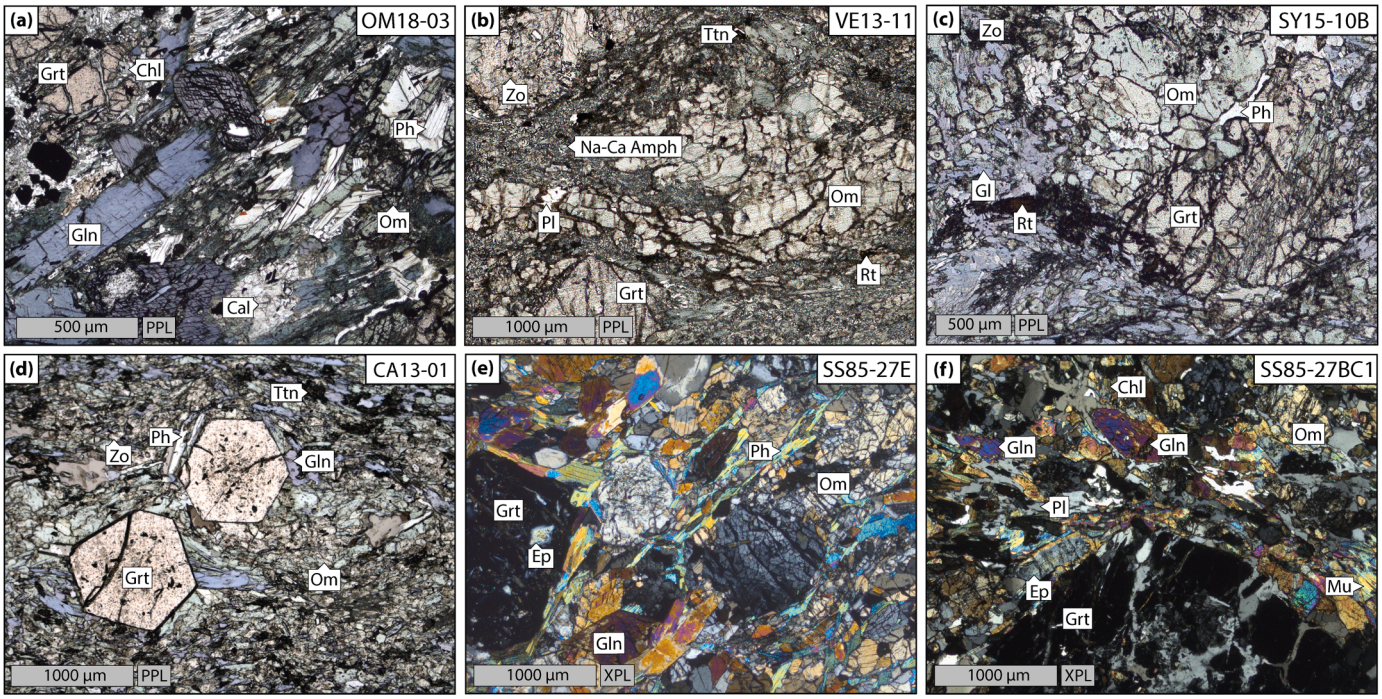

Fig. 1. Representative thin section photomicrographs of select samples. (a) Retrogressed and foliated eclogite OM18–03C from As Sifah, Oman, showing strongly fractured garnet and calcite clots. (b) Foliated amphibolite–eclogite VE13–11 from Puerto Cabello, Venezuela, with bands and clots of omphacite in a symplectic matrix (c) Coarse and unfoliated blueschist–eclogite SY15–10B from Syros, Greece. (d) Fine grained and foliated matrix with euhedral garnet inblueschist–eclogite CA13–01 from Ring Mountain, California. (e) Core eclogite SS85–27A from Punta Balandra, Dominican Republic, with moderately foliated epidote rich foliation. (f) Rind eclogite SS85–27BC1 from Punta Balandra, Dominican Republic with fracture but euhedral garnet in well foliated finer matrix. Mineral abbreviations are after Whitney and Evans (2010).

abundant divalent cations in these garnets) do not exhibit clear oscillations. In places, the Ca zoning hints at patterns parallel to oscillations in Mn, but the dominantly patchy and non-concentric Ca distribution may record kinetic inhibition and chemical disequilibrium, as suggested for other rocks (e.g., George et al., 2018).

Mn zoning in garnet from sample OM18–03C typifies the form of oscillatory zoning investigated in this study. It is present across the outermost 300–500 µm of garnet (Fig. 2a), rim-wards of a broad core-to-mantle decrease in the spessartine content. Garnets in OM18–03B, collected from the same location (2 m apart) and with an equivalent assemblage, contain narrower oscillatory regions and a different sequence of peaks and troughs (Fig. 2b; SM 3). For a given Oman hand sample, equivalent oscillations can be tracked among garnet grains, and in both OM18–03B and −03C the onset of short-wavelength oscillations is associated with an increase in average spessartine and grossular contents (by ~1 mol.% and ~11 mol.%, respectively) that continues to

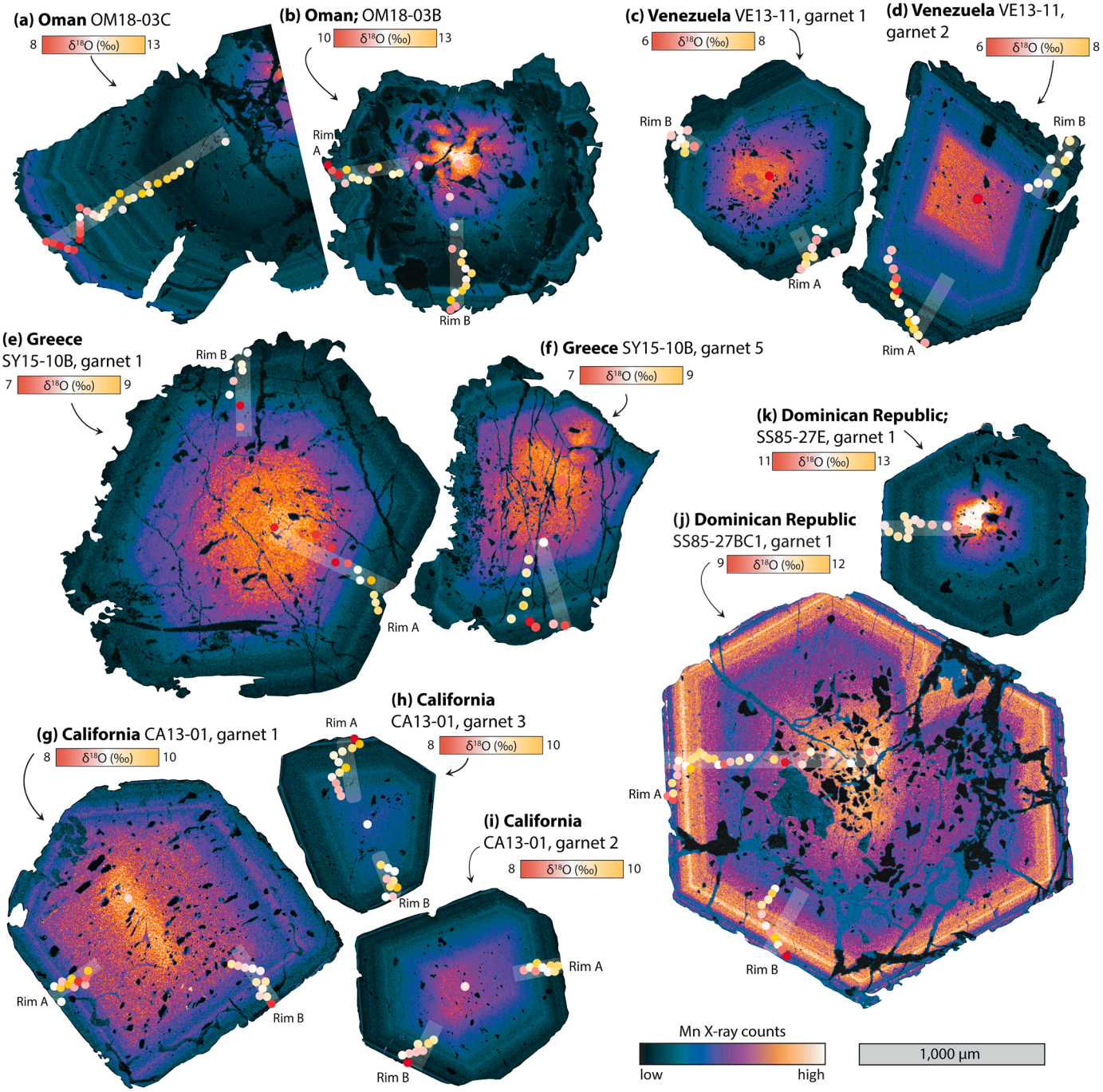

Fig. 2. X-ray count maps of Mn zoning, and locations and O-isotope compositions for analyzed garnets from a suite of exhumed *HP–LT* subduction zones. (a) and (b) Garnets from samples collected meters apart in outcrop from As Sifah, Oman; (e) and (d) two garnets from the same thin section from Puerto Cabello, Venezuela; (e) and (g) two garnets from the same thin section from Syros, Greece; (g), (h) and (i) garnets from one thin section from Ring Mountain, California; (j) and (k) eclogite rind and core garnets, respectively, from Punta Balandra, Dominican Republic. X-ray maps show relative counts in garnets (matrix regions have been masked but inclusions in garnet are preserved), are scaled to a single length scale, and are cropped at the outermost rim of garnet. Spots give location and SIMS points (scaled 2x actual size) and are colored according to their $\delta^{18}O$ value using color scales specific to each grain.

increase towards the rim, and a decrease in the average almandine content (Fig. 2a, b; SM 3). The Mn maps in all Venezuelan garnets from VE13–11 exhibit single, ~35 µm-wide mantle peaks succeeded by three near-rim peaks that contain lower Mn and Fe and higher Mg (Fig. 2c, d; SM 3). In the three Greek garnets from SY15–10, all grains exhibit a single 50–70 µm wide oscillation in Mn content (Fig. 2e, f; SM 3). In Californian garnets from CA13–01, oscillations occur in the rim-most 200–250 µm (Fig. 2g–i). In the outermost 30 µm of Californian grains, there is a euhedral and now partially-resorbed rim of higher spessartine and grossular (by ~2 mol.% and ~1 mol.%; Fig. 2h, i, SM 3) and lower pyrope (by ~1 mol.%; SM 3); similar rims are not observed in garnets from other settings. In the two mapped Dominican Republic rind garnets from SS85–27BC1, 10–50 µm-wide oscillations—again equivalent across different grains within a single thin section—are superimposed on a near-rim shoulder in Mn and a narrow outer-rim region containing lower Mg and Ca, and high Fe content (Fig. 2j; SM 3). In the smaller garnet from the core of the same block (sample SS85–27E), two ~100 µm-wide Mn peaks are identifiable (Fig. 2k, SM 3).

In any given hand sample, major element oscillations are equivalent between garnets: individual oscillations with similar amplitudes and wavelengths have common radial positions from garnet rims, indicating that they formed simultaneously in systems chemically equilibrated at least at the cm-scale at any given time (e.g., George and Gaidies, 2017); this does not imply equilibration over the core-to-rim duration of garnet growth. Converse to this finding of apparent hand sample scale equilibration at any given time, garnets from samples collected across the meter-scale (e.g., Oman and the Dominican Republic) exhibit differences in the precise positioning and number of fine-scale oscillations, indicating equilibration did not extend to these length scales. However, for each of these settings, grain-scale step changes in *average* elemental composition are ubiquitous across this length scale, suggesting that any change in major element chemistry was progressive across a rock volume/outcrop.

Corresponding LA–ICP–MS maps of trace elements in garnet from OM18–03 reveal a diverse suite of zoning patterns, variably correlated with the distribution of major elements. Light to heavy REEs (L–HREE) and Y exhibit oscillations that are spatially coincident with those preserved in Mn, but sometimes differ in terms of whether they are positively or negatively correlated (Fig. 3a–c; SM 4). With the exception of Lu, oscillations are generally less pronounced from HREE to LREE, and Y and HREE indicate that elemental oscillations occur more core-ward than revealed by the major-element EPMA maps (Fig. 3a, b; SM 4).

Changes in the oxidation state of the reactive bulk composition modifies the Fe^{3+}–Al octahedral site ratio incorporated into garnet during growth (a substitution less dependent on temperature, pressure, pH, and salinity in garnets containing X_{grs}<0.4; Jamtveit et al., 1995). The andradite content of garnet (X_{And}) in this study is <1–5 mol.%, consistent with the typical range reported in *HP–LT* metamorphic garnet (cf. Gerrits et al., 2019). Garnet in CA13–01, SS85–27BC1, SS85–27E, VE13–11, and SY15–10 exhibit no systematic Al or andradite zoning across regions of elemental oscillations or outermost rims (Fig. 4c–k; SM 3). However, both grains from Oman exhibit near-rim concentric increases in Al content (Fig 3e; SM 3), and associated rim-ward declines in the andradite content, from 4 mol.% to 2 mol.% (Fig. 4a, b). These

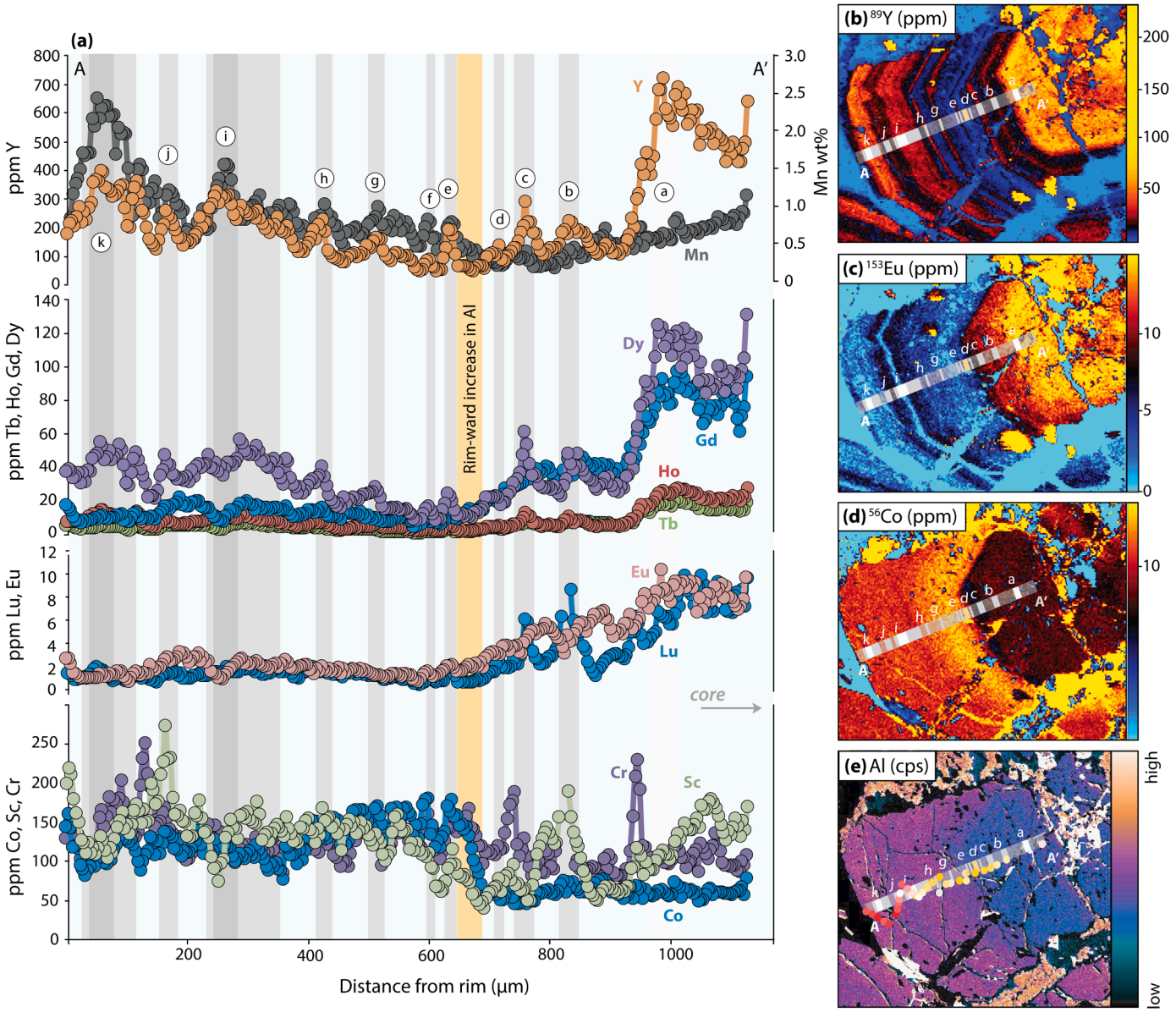

Fig. 3. Trace element and Al zoning in garnet 1 from sample OM18–03C. (a) LA–ICP–MS trace element profile along transect in Fig. 1A. (b), (c), and (d) LA–ICP–MS maps of Y, Eu and Co zoning, respectively. (e) X-ray map of Al content, showing position of profile in (a) and of SIMS points. gray vertical bands locate oscillatory peaks identified in Y, and their positioning is indicated in the transect in (b)–(d).

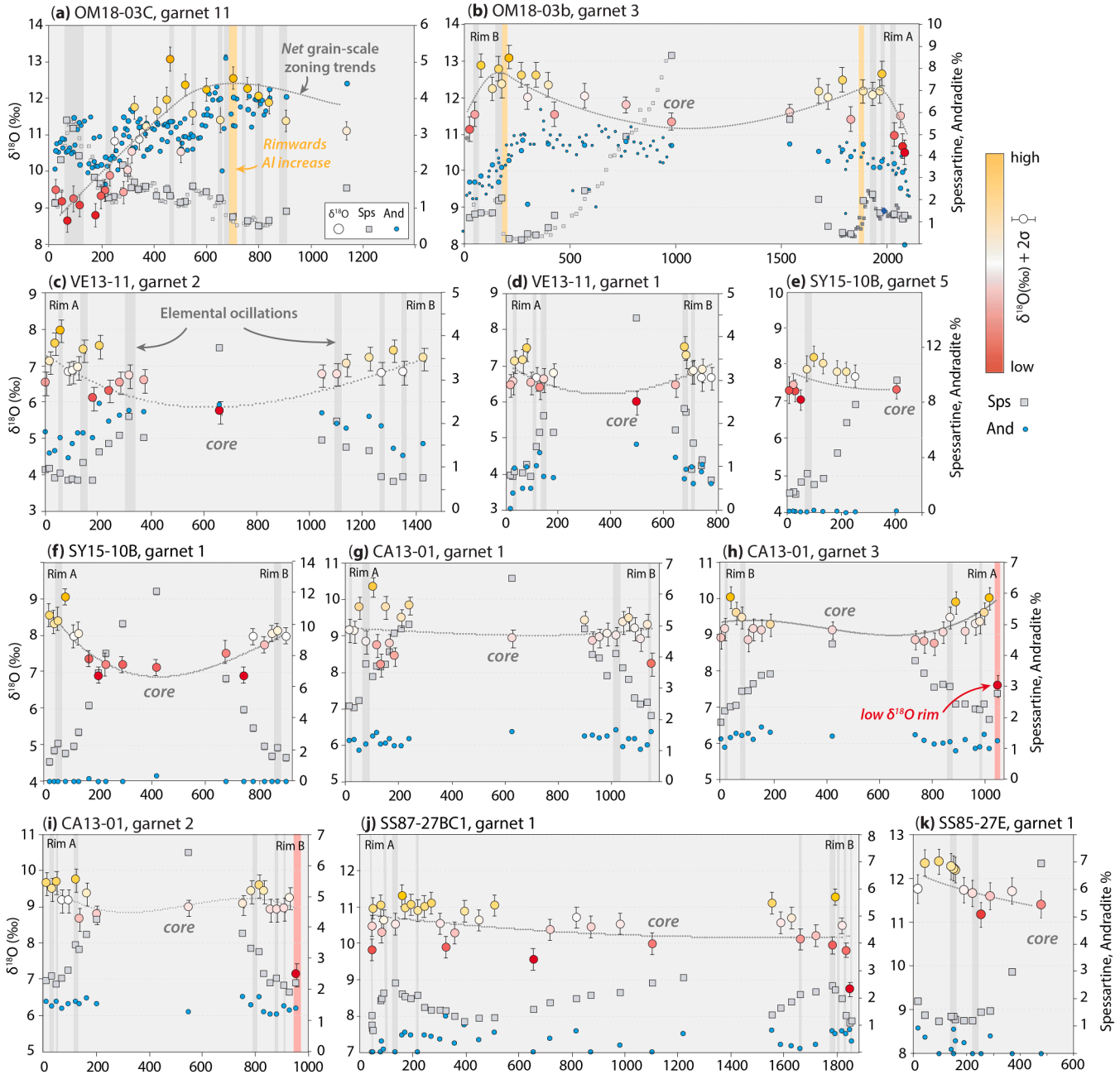

Fig. 4. Oxygen isotope and elemental zoning across garnet plotted from rim to rim. (a)–(k) lettering scheme as for Fig. 1. $\delta^{18}O$ values (circles) for a given grain across opposing rims are plotted with respect to a core point. $\delta^{18}O$ points are colored as in Fig. 2, and error bars represent ± 1σ uncertainty obtained by propagation of the internal error, the error on mass fractionation correction, and the error on the matrix effect correction. A third-order polynomial is fit to $\delta^{18}O$ to highlight the net core-to-rim zoning (dotted lines). Squares show spessartine content used for matrix correction (small gray squares in (a) and (b) are high-sampling resolution profiles across same transect). Small blue circles show calculated andradite content. On all plots, gray shaded region denotes the position of positive oscillations (i.e. peaks) from Fig. 2, yellow bands in (a) and (b) and red bands in (h) and (i) indicate where elemental and isotopic changes are coupled.

boundaries are coincident with pronounced changes in average Mn, Fe, and Ca content (SM 3). A change in concentration of redox-sensitive trace elements (V, Co, Eu and Cr) also coincides with this mapped change in Fe^{3+}–Al substitution (Fig. 3c–e; SM 4). Though only subtly expressed on linearly scaled plots of concentration, this boundary also marks an inflection point across which the average rim-ward gradient in Y, REE, and Sc inverts from negative to positive (Fig. 3a).

3.2. Oxygen isotope zoning in garnet

The positioning of SIMS oxygen isotope analysis transects were chosen based on the Mn zoning and are shown as spots in Fig. 2 and core–rim profiles in Fig. 4. Full data for individual measurements and associated matrix corrections are provided in SM 5.

The core $\delta^{18}O$ (with 2SD) in garnet from different locations varies: 5.7 ± 0.35 ‰ in Venezuela, 7.2 ± 0.27 ‰ in Greece, 8.9–9.1 ± 0.27 ‰ in California, 10–11.5 ± 0.27 ‰ in the Dominican Republic and 10.5–11.3 ± 0.3 ‰ in Oman. These variable departures from a primary

MORB value ($\delta^{18}O$ ~5.5 ‰) are interpreted to reflect inheritance of the $\delta^{18}O$ signature derived from variable degrees of low-*T* hydrothermal alteration of oceanic crustal protoliths, rather than reflecting prograde metamorphic processes (Russell et al., 2013, Putlitz et al., 2000). A contribution to the differences in absolute near-core $\delta^{18}O$ may also derive from *T*-dependent isotope fractionation at the variable *T* of incipient garnet growth in each rock (e.g., Kohn et al., 1993; Vho et al., 2020). Rim-ward of cores, distinct $\delta^{18}O$ zoning patterns incorporate features preserved over two distinctly different wavelengths.

At the sub-grain scale (100–500 μm), garnets exhibit intragrain $\delta^{18}O$ variation characterized by 50–300 μm-wide ≲1–2 ‰ 'saw-tooth' vacillations (i.e., fluctuations less regular than elemental oscillations) that exceed the internal uncertainty on individual analyses (0.27–0.34 ‰; Fig. 4). For example, across one core-to-rim profile for a garnet from the Dominican Republic (SS85–27BC1), internal $\delta^{18}O$ variation defines three coherent ~11 ‰ peaks in $\delta^{18}O$ across a radial distance of ~1200 μm, with $\delta^{18}O$ repeatedly returning to values of ~9.5 ‰ rim-ward of each peak (Fig. 4j). Unlike the oscillatory zoning in major elements, which is relatively uniform across and among grains from single thin sections, this intragrain oxygen isotope zoning in garnet differs among garnets from the same thin section; for example, in SY15–10B garnet 5, $\delta^{18}O$ exhibits a gentle increase from the core then a sharp decrease ~100 μm from the rim (Fig. 4e), whereas $\delta^{18}O$ in SY15–10B garnet 1 exhibits only average increases towards the rim (Fig. 4f). Average $\delta^{18}O$ in rims of all California garnets are similar (9 ± 1 ‰), but the outermost rim point of one profile in each garnet has a $\delta^{18}O$ that is ~2 ‰ lower than the adjacent point (Figs. 2g–i and 4g–i). Intra-grain zonation in Californian garnets is sometimes symmetrical about the core but can also be asymmetric, and differs between grains. For example, CA13–01 garnet 1 (Fig. 4g) exhibits asymmetry across the core, with one rim exhibiting only minor spot-to-spot change with a range of ~1 ‰ and the other displaying internal variation up to ~2 ‰. In contrast, some across-core symmetry is present in other grains of the same thin section: both mantle/rim regions of CA13–01 garnet 3 contain a $\delta^{18}O$ increase of ~1 ‰ then steep decrease of a similar magnitude. A secondary $\delta^{18}O$ increase of ~1 ‰ and then a steep near-rim ~2 ‰ decline in one rim this same grain suggests this symmetry does not persist over the whole of the core-to-rim (in contrast to major element zoning).

In samples from Venezuela, Greece, and the Dominican Republic, these internal and short-wavelength $\delta^{18}O$ vacillations are superimposed on flat (~0 ‰) to a 1–1.5 ‰ overall *net* $\delta^{18}O$ increase across cores to rims of garnet (Fig. 4c–f, j, k). Garnets from California also exhibit uniform to slightly increasing interior $\delta^{18}O$, excluding the anomalously low $\delta^{18}O$ points in the outermost rims (Fig. 4g–i). From the 11–12 ‰ core value of Oman garnet there is a similar net increase to values of 12–13 ‰. Then, rim-ward of these maxima, $\delta^{18}O$ vacillations in OM18–03B and −03C are superimposed on a longer wavelength net decrease in $\delta^{18}O$ of 2.5–4 ‰ (Fig. 4a, b), which flattens in the outermost rim (Fig. 4b). Garnets from Oman, derived from similar samples collected 2 m apart, have rim isotopic compositions that differ by ~2 ‰.

3.3. Covariance (or not) among $\delta^{18}O$ and cation zoning

As the most pronounced component in which oscillations are documented, the Mn content is hereafter used as the principal comparative element to determine if isotopic changes are spatially associated with elemental changes in garnet. Analysis of linear covariance between $\delta^{18}O$ and spessartine content suggests no (positive or negative) coupling between the two datasets across oscillatory zoned regions of any grain (Table 2). Correlation coefficients (r-values) calculated for the $\delta^{18}O$ and corresponding spessartine were also calculated along each profile. Generally, these exhibit moderate and negative r-values. In most cases, these are not significant at the 95 % confidence level, but in the cases of OM18–03C and SY15–10B there is a statistically significant anti-correlation (Table 2); these likely result from the strong fractionation-controlled core-to-rim decrease in Mn content and slight net core-to-rim increases in $\delta^{18}O$. Correlations between the magnitude of fluctuations from point to point (which may be expected to be significant if the two datasets vary at the same wavelength) are not significant in any grain.

Principal component analyses (PCA) performed for combined mantle and near-rim regions of grains from a given locality (details provided in SM 3) similarly highlight the absence of any systematic covariance between spessartine and $\delta^{18}O$ (Fig. 5); in addition, no other garnet end-member consistently exhibits correlation with $\delta^{18}O$. As with statistical approaches, empirical assessments of the covariance between elemental maps and isotopic spots across oscillatory rims in Fig. 2 indicate no spatial coincidence between the positioning of elemental oscillations and internal short-wavelength intragrain variation of $\delta^{18}O$.

The only correlative record between oxygen isotope compositions and elemental compositions occurs in garnet from Oman and at the very outermost rims of Californian garnet. In the Oman samples, long wavelength, rim-ward decreases in $\delta^{18}O$ are spatially coincident with declines in the andradite content and pronounced changes in average major and trace element concentrations (Fig. 4a, b; SM 3, 4). Andradite reference standards were monitored during analyses (and calibrations checked) and suggest that the matrix bias effect had negligible impact on this change; at the X_{And} of relevance (<0.04) the additional $\delta^{18}O$ matrix correction is ~0.2 (consistent with that calibrated Martin et al., 2014). Based on LA–ICP–MS maps of OM18–03C, the position of this significant change in garnet composition (Fig. 3a) is not coincident with the core-most radius at which oscillations are detectable in the Y and REE content (i.e., small-wavelength elemental vacillations are evident in both isotopically distinct core and rim domains). In California, the sharp decrease in $\delta^{18}O$ in the outermost 30 μm is spatially correlated with a thin, partially resorbed high-Mn rim, but there is no associated X_{And} change at this boundary.

Table 2
Covariance and correlation between $\delta^{18}O$ and corresponding spessartine content at the 95% confidence level for garnets in Fig. 1 and 2. Results for both raw recalculated analyses and for the difference between adjacent analyses (i.e., the change in these values).

Sample	Grain	Spessartine & $\delta^{18}O$					Change in Spessartine & $\delta^{18}O$				
		N	CoVar	r-value	P	95%	N	CoVar	r-value	P	95%
OM18-03C	g1	30	-0.01	-0.68	5×10^{-5}	sig.	29	0.00	-0.30	0.22	not sig.
OM18-03B	g3	28	0.00	-0.24	0.23	not sig.	26	0.00	-0.25	0.22	not sig.
VE13-11	g1	18	0.00	0.21	0.40	not sig.	17	0.01	0.43	0.08	not sig.
VE13-11	g2	22	0.00	-0.28	0.20	not sig.	20	0.00	0.39	0.09	not sig.
CA13-01	g3	17	-0.00	-0.01	0.97	not sig.	16	0.00	-0.09	0.87	not sig.
CA13-01	g2	22	0.00	0.16	0.47	not sig.	21	0.00	0.23	0.45	not sig.
CA13-01	g1	21	0.00	-0.38	0.09	not sig.	19	0.00	-0.27	0.31	not sig.
SS85-27BC1	g1	37	-0.00	-0.11	0.55	not sig.	35	0.00	0.02	0.92	not sig.
SS85-27E	g1	13	-0.00	-0.45	0.12	not sig.	12	-0.00	-0.29	0.36	not sig.
SY15-10B	g5	10	0.00	0.32	0.38	not sig.	9	0.00	-0.25	0.51	not sig.
SY15-10B	g1	17	-0.02	-0.77	3×10^{-4}	sig.	16	0.00	-0.16	-0.56	not sig.

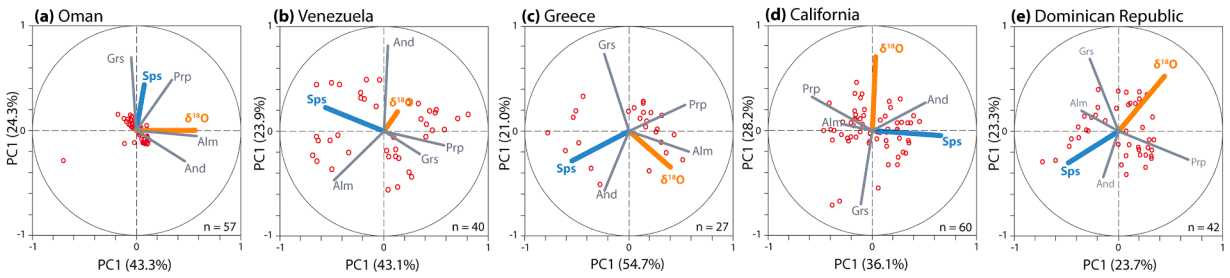

Fig. 5. Results of principal component analyses. (a)–(e) Log-transformed and scaled coordinate values for PC1 v. PC2 loadings, and corresponding scores and eigenvectors for data from all garnets assessed with SIMS. The number of analyses included in each PCA are shown, and the percentage on each axis represents the total variance explained by that component.

3.4. Summary of elemental and oxygen isotopic zoning observed in the HP-LT garnets

1. Short-wavelength oscillations are present in garnet mantle and rim regions in Mn, and Mg in some samples. Where L–HREE and Y were also mapped, these elements covary with Mn. Euhedral elemental zoning patterns are axisymmetric in all grains studied and are equivalent for garnets sampled centimeters apart.
2. Unlike the elemental zoning patterns, short-wavelength core-to-rim vacillations in $\delta^{18}O$ (observed in all garnets) reach a maximum range of ~2 ‰, are not always axisymmetric and vary among grains separated by mm-to-cm length scales. Qualitative analysis and PCA reveal zero spatial coincidence (coupling) or covariance among short-wavelength elemental oscillations and $\delta^{18}O$ variations.
3. In the Oman garnets, long-wavelength variations in chemistry (upon which the shorter-wavelength records are superimposed) are revealed by grain-scale Al (andradite) variation and systematic changes in $\delta^{18}O$ with onset in mantle regions and which are not observed in garnets from any of the other samples. This zoning is coupled to variation in other redox-sensitive elements (V, Co, Eu, Cr), in addition to trace elements/REEs (e.g., Y, Dy, *Sc*). In garnet from California, there is only coupling between $\delta^{18}O$ and major elements in very narrow outer rims.
4. Garnets from the Dominican Republic, Greece, and Venezuela show negligible (<1 ‰) *net* core-to-rim $\delta^{18}O$ variation.

4. Discussion

Results presented here demonstrate the coexistence of short-wavelength elemental oscillations and saw-tooth intra-grain oxygen isotope variations in *HP-LT* garnet, but suggest that these signals are decoupled. There is no evidence in our data to demonstrably link oscillatory elemental zoning in *HP–LT* metabasic garnet to pulsed infiltration of isotopically-distinct grain boundary fluids that are out of equilibrium with the rock and which buffer garnet chemistry, as has been suggested for some shallower fluid-rich settings (e.g., Jamtveit et al., 1995; Yardley et al., 1991) and eclogitic vein garnet (e.g., Spandler et al., 2011; Angiboust and Raimondo, 2022).

The *net* core-to-rim variation in all garnet from the Dominican Republic, Venezuela, and Greece (and California, excluding the outermost rim point) is $\leq 1 \pm 0.3$ ‰. Such modest (0.2–1 ‰) core-to-rim increases in the $\delta^{18}O$ of garnet have been previously shown to result from closed-system mineral fractionation, dehydration reactions, and fluid loss over a temperature evolution of 100–200 °C (Kohn et al., 1993; Vho et al., 2020). The net core-to-rim variation documented in these garnets is therefore consistent with crystallization in broadly closed systems.

Conversely, in garnets from Oman, a dramatic change in major and trace element concentration is coupled with a mid-mantle 2.5–4 ‰ decrease in $\delta^{18}O$, a magnitude exceeding that modelled for prograde garnet crystallization in a closed system (Kohn et al., 1993; Vho et al., 2020). These coupled, grain-scale zoning records are interpreted to reflect opening of the grain boundary network to externally-derived, isotopically-, and chemically-distinct and buffering fluids (Fig. 6). Given the oscillatory elemental zoning incorporated after this infiltration event, towards the garnet rim, it is considered to have been synchronous with ongoing prograde garnet growth.

The coupling between low-$\delta^{18}O$ and high-Mn domains in rims of Californian garnet from one locality studied here (Ring Mountain) has also been documented by Errico et al. (2013) and Cruz-Uribe et al. (2021). In these previous studies, this near-rim (outermost ~50–100 μm) decline in $\delta^{18}O$ has been interpreted to reflect external fluid infiltration at the end of prograde garnet growth, potentially marking the point at which the block was removed from the slab, thus allowing new infiltration of serpentinitic mélange fluids (Errico et al., 2013; Page et al., 2014; Cruz-Uribe et al., 2021). If (as we consider likely) the near-rim isotopic zoning in our Californian grains reflect a similar process of buffering fluid-infiltration, the timing of fluid infiltration may be in marked contrast to mid-growth timing of fluid infiltration in the Oman grains.

Below, we discuss: (a) alternate mechanisms by which oscillatory elemental zoning may be incorporated in garnet during prograde growth; (b) the potential origin of the small-wavelength $\delta^{18}O$ vacillations observed in all samples; and (c) the magnitude, composition, and source of fluids that buffer garnet compositions during growth in Oman.

(a) Potential origin of the short-wavelength elemental oscillations

Spatially associated but decoupled short-wavelength $\delta^{18}O$ variation and elemental oscillations in garnet require that the driver of each short-wavelength zoning pattern (elemental v. oxygen isotopic) act simultaneously, yet possibly independently. The apparent decoupling of the records is inconsistent with the notion that fluctuating elemental concentrations are driven by intermittent pulses of fluid-buffered change to the effective grain boundary chemistry, as proposed by Jamtveit et al. (1995), Yardley et al. (1991), Moore et al. (2013), and Tamblyn et al. (2020). Discrete, long-range fluid transfer events, as proposed to explain the longer-wavelength zoning feature in the Oman garnets, seem to exert little influence on the underlying process(es) driving the elemental oscillations, which are recorded both prior to and after first evidence of open system behavior (Figs. 3 and 4). The consistency of the radial positioning and amplitude of major element oscillations between grains of a given sample indicate that nutrient uptake was equilibrated (and garnet incorporated the same chemical composition at any given time) across at least the cm scale (e.g., George and Gaidies, 2017), in pronounced contrast to cross-porphyroblast disequilibrium in short-wavelength $\delta^{18}O$ zoning in the same grains.

Repeating elemental oscillations in garnet have been attributed to several intrinsic (kinetic) and extrinsic (geodynamic) controls. They have been interpreted, for example, to result from complex mechanical cycling of material across and along the slab–mélange interface. In such cases, oscillations form as an equilibrium response to rock-scale *P–T*

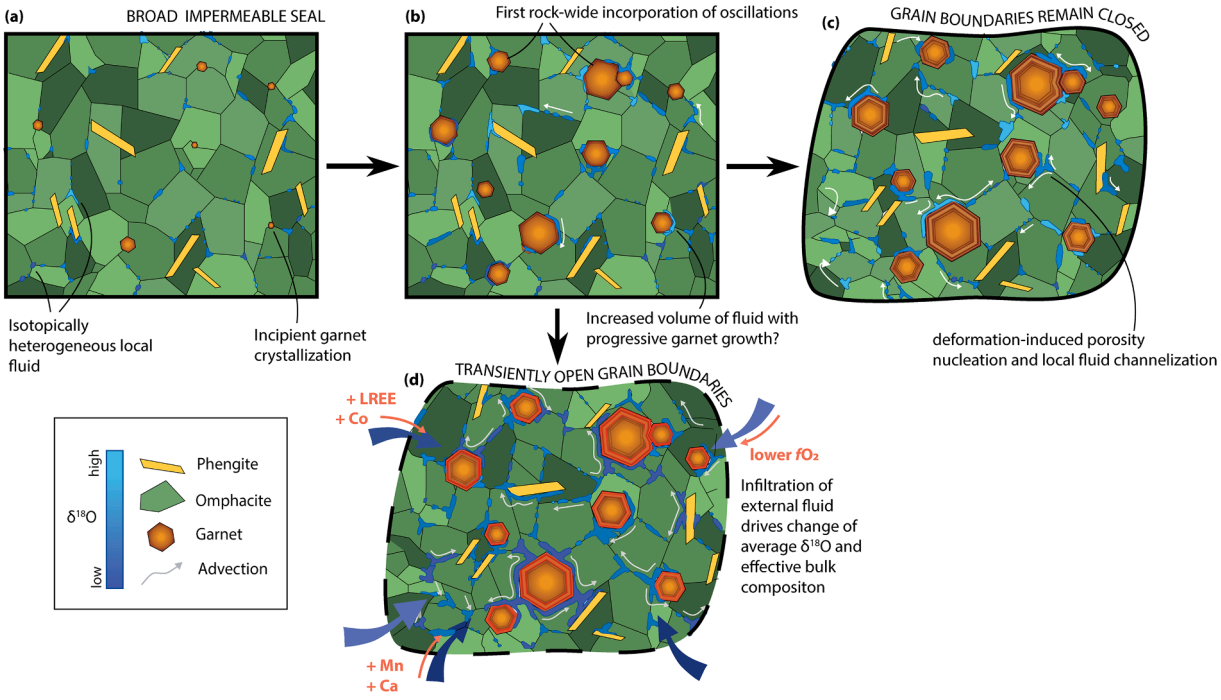

Fig. 6. Conceptual model for the migration of grain boundary fluid during garnet growth in low-porosity *HP–LT* metabasites. (a)–(c) Typical rock-wide evolution with non-interconnected and isotopically heterogenous fluid, involving local porosity nucleation, micro-channelization, and fluid migration. (d) Less common scenario in which grain boundaries are transiently opened, permitting ingress of external, chemically, and isotopically distinct, fluids that buffer a change in the stable mineral (i.e., garnet) composition.

fluctuations (e.g., García-Casco et al., 2002; Blanco-Quintero et al., 2011; Tan et al., 2020), consistent with our constraints on their simultaneous incorporation in different grains. However, evidence from California suggests that distinct *HP–LT* eclogite blocks may have had a common source in an underplated slab (Cisneros et al., 2022), and that garnet growth at eclogite-facies conditions likely occurred prior to free incorporation in the mélange. Whether an origin in equilibrium responses to rock-scale *P–T* fluctuations is applicable to other samples in this study remains debatable. Preservation of steep chemical gradients in Mn zoning may also preclude physical processes that operate over tens of millions of years, because diffusion would be expected to homogenize gradients within several hundred Kyr, faster than the timescales of associated tectonic processes (Viete et al., 2018). Alternatively, dissolution and reprecipitation processes can drive cyclic incorporation of highly fractionating elements, either in response to partial resorption (Kulhánek and Faryad, 2023) or short-duration pressure pulses associated with seismic cycles (Viete et al., 2018). However, the oscillations assessed here are euhedral and do not generally exhibit non-parallelism expected for resorption (e.g., Pyle and Spear, 1999), questioning the potential role of dissolution–reprecipitation.

Chemical oscillations have also been linked to intermittent major and/or accessory mineral breakdown (e.g., Konrad-Schmolke et al., 2008; Hyppolito et al., 2019; Kulhánek and Faryad, 2023). This would require rapid rock-wide redistribution of liberated chemical components, suggested by Kulhánek and Faryad (2023) to be closely tied to the continuous availability of a fluid medium. This may be at odds with the emerging picture of limited connectivity through the grain boundary network at high pressure (e.g., Mibe et al., 2003; Angiboust and Raimondo, 2022). However, Konrad-Schmolke et al. (2023) recently proposed a mechanism whereby elemental fluctuations result from changing transport properties of the matrix, with garnet peaks and troughs representing switches between equilibrium and transport-limited kinetic scenarios, respectively. This may account for the (fluctuating) scales of elemental equilibration observed in our garnets; however, it is not clear how fluctuating rock permeability (and therefore potential for grain boundary advection) in this model—driven, for example, by compaction and devolatization cycles and/or seismicity and externally-imposed dilatancy—may relate to the short-wavelength isotopic variations, which are decoupled from the oscillatory elemental zoning.

Though many published examples of oscillatory zoning of REE+*Y* in *HP–LT* garnet have not simultaneously considered major element zoning (including Konrad-Schmolke et al., 2023), samples in this study indicate that the two elemental zonation patterns can be spatially and therefore genetically related. In some cases, the apparent absence of major element oscillatory zoning may be because oscillations are too subtle (in space or magnitude) for analytical detection or because of homogenization of steep chemical gradients by post-growth diffusion (e.g., George et al., 2021). In samples investigated here, the presence of equilibrated oscillations in highly partitioning, low concentration elements that have both rapid (i.e., Mn) and relatively slow (e.g., Y and HREE) diffusivities may suggest that it is the effective concentration in the grain boundary rather than intragranular kinetic properties that control incorporation (cf. Konrad-Schmolke et al., 2023). Such concentration changes could be driven, for example, by periodic rock-wide changes to element solubility in the grain boundary resulting from modest *T* changes (Tsay et al., 2017) or the carbonate–bicarbonate or CO_2–H_2O concentrations of the fluids, which has been shown to dramatically alter length scales of equilibration (Carlson et al., 2015).

(b) Origin of the short-wavelength oxygen isotope vacillations in all samples

In all samples studied, intra-garnet $\delta^{18}O$ variations with magnitudes of 1–2 ‰ point to temporal heterogeneity in the isotopic composition of the grain boundary in systems that do not obviously record open-system buffering conditions (with the exception of the unique events recorded in the case of Oman and California) over the core-to-rim duration of garnet crystallization. In contrast to axi-symmetry in elemental zoning, cross-porphyroblast asymmetry of the $\delta^{18}O$ vacillations in some garnets

(Fig. 3), in addition to grain-to-grain heterogeneity in $\delta^{18}O$ zoning, alludes to significant mm- to cm-scale spatial heterogeneity in the distribution of ^{16}O v. ^{18}O throughout the duration of mineral growth.

From where then do these intra-grain and cm-scale spatiotemporal heterogeneities in $\delta^{18}O$ arise? As hypothesized by Russell et al. (2013), who documented similar scale isotopic fluctuations in orogenic eclogites, saw-tooth variations may indicate fluxing of higher and lower $\delta^{18}O$ fluids through the grain boundary network, derived from alternating (external) sedimentary and mafic sources. Such a scenario would require transient passage of fluids that do not impart a lasting isotopic signature in the rock (i.e., are rock buffered) yet maintain fluid compositions that are out of equilibrium (i.e., not rock buffered) over their transfer distances, which are unknown but may be significant. Moreover, a scenario of garnet crystallization at high pressure while attached to the down-going slab rather than the mélange, would require underlying sedimentary sources to feed the slab-normal (or up-dip) migration of relatively high-$\delta^{18}O$ fluids, which is a difficult architecture to account for. With the apparent difficulty of explaining short-wavelength $\delta^{18}O$ variations (decoupled to short-wavelength elemental zoning) in terms of external fluid ingress, we hypothesize potential explanations for the fluctuations in $\delta^{18}O$ that are internal to the rock volume.

Experimental constraints suggest that high dihedral angles (62°–68°) facilitate the evolution of isolated fluid pockets in *HP* rocks (Mibe et al., 2003). In such systems, heterogeneous, rock-wide variations in $\delta^{18}O$ of the grain boundary fluid may develop in a non-interconnected porosity in response to: (1) spatially variable reaction–dehydration extent across the mm-to-cm scale; (2) local fractionation; or (3) evolution of extreme disequilibrium. Abrupt and spatiotemporally heterogenous breakdown of low-*T* phases (e.g., lawsonite or albite) may also drive local heterogeneity in fluid $\delta^{18}O$. Notably, the maximum range in internal short-lengthscale $\delta^{18}O$ variation in garnet (~2 ‰) is significantly higher than the maximum intragrain variation documented in contact and regional metamorphic settings by Ferry et al. (2014). This greater isotopic heterogeneity may result from the reduced interconnectivity of *HP–LT* systems compared to lower-*P* metamorphic settings.

Free fluids within the rock volume may become transiently and variably interconnected during deformation-induced dilatancy and/or porosity development (e.g., Holness, 1993), a process potentially enhanced along grain boundaries with favorable crystallographic misorientations; such episodic changes may result in isotopic variations across the surfaces of growing garnet. Upon this 'opening' of non-interconnected porosity, grain-scale channelization of aqueous fluid between domains containing discrete $\delta^{18}O$ may be driven by local gradients in fluid pressure and isotopic potential gradients that are then maintained during coupled reaction–transport processes (Plumper et al., 2017). Fluid–solid dihedral angles may also vary locally (e.g., Holness, 1993), particularly if large differential stresses are sustained across grains (Tajčmanová et al., 2014), resulting in heterogeneous transfer of fluid that is also modified by porosity–permeability changes and fluid production during volume changes associated with prograde metamorphic reaction (Fig. 6a–c; e.g., Plumper et al., 2017, Bovay et al., 2021). Alternatively, as with changes to the stress field in shallow systems (e.g., Elkhoury et al., 2006), down-dip transfer of dynamic seismic effects to garnet-stable parts of the subduction zone may induce episodes of enhanced permeability.

Short-wavelength $\delta^{18}O$ vacillations may therefore record highly localized (mm- to cm-scale) changes to porosity–permeability linked to episodic processes in the dynamic subduction zone environment. This scenario is consistent with the hypothesis that old $^{40}Ar/^{39}Ar$ ages result from accumulation of radiogenic Ar under closed system conditions (e.g., Warren et al., 2011; Smye et al., 2013) and are consistent with reports of isolated fluid pockets at *HP–LT* conditions (Angiboust and Raimondo, 2022). It may also imply that a crustal scale recycling budget dominated by volatile solubility in serpentinite may be supplemented with volatiles preserved in stagnant—yet spatially and temporally heterogeneous—grain boundary pore space of mafic eclogite and blueschist.

(c) Buffering of elemental and isotopic signatures at long length scales by external fluids in Oman

Our data provide no evidence in support of models for development of elemental oscillations via repeated episodes of infiltration of fluid in pronounced disequilibrium with the rock. However, if infiltrating fluids had similar chemical and isotopic compositions to the country rock (i.e., were equilibrated) or equilibrated with the oxygen already in the rock volume through which it passes, external fluid ingress may leave no observable isotopic signature. In contrast, samples from Oman provide clear, spatially-coupled evidence for significant modification to the effective bulk composition during the middle of garnet growth via infiltration of an isotopically- and chemically-distinct external (to the rock volume) fluid (Fig. 6d). The discrete, 2–4 ‰ near-rim declines in $\delta^{18}O$ in the Oman garnet are also comparable to changes interpreted to result from open system metasomatism in previous studies (e.g., Russell et al., 2013; Rubatto and Angiboust, 2015; Martin et al., 2014; Bovay et al., 2021; Cruz-Uribe et al., 2021). At this compositional–isotopic boundary, the corresponding decrease in the calculated andradite component, by 2–3 mol.%, indicates that open system fluid infiltration during garnet mantle–rim growth may have been associated with a reduction of the reactive bulk fO_2 relative to the growth environment for core regions. A rock-wide increase in $Eu^{2+}/\sum Eu$ linked to reduction of the reactive bulk fO_2 may also explain the documented decline in Eu concentration at this boundary (Fig. 2c).

Owing to their large partition coefficients in garnet, steep decreases in the concentration of MREE and HREE rim-ward of core regions are expected to result from Rayleigh fractionation, with closed chemical systems yielding strongly depleted rims. However, in addition to an enrichment of the reactive bulk composition in Ca and Mn, the decline in andradite and $\delta^{18}O$ in Oman garnet is accompanied by subtle rim-ward increases in REE content. If this change is related to protracted fluid infiltration, these data may be consistent with recent experiments that have suggested that REEs can be mobilized in aqueous fluids at high *P* (Tsay et al., 2017). Experimental constraints also attest to significant fluid mobility for Cr (Kogiso et al., 1997; Kessel et al., 2015), in agreement with a fluid-buffered increase in the average Cr concentration in the mantle–rim regions of the Oman garnets (SM 4). Walters et al. (2022) suggested that Co budgets are dominated by reactions among Fe–Mg silicate phase; in our rocks, a buffered increase of the Co concentration (Fig. 3a) in the grain boundary by the proposed fluid infiltration event suggests significant Co mobility in subduction zone fluids.

4.1. Source and volume of external fluids recorded in the Oman garnets

Quantitative isotopic and thermodynamic modeling was conducted to explore the volume of fluid required to drive the observed isotopic changes in the Oman garnets. Although the bulk rock oxygen isotope composition of the Oman eclogites is unknown, it can be reconstructed using mineral $\delta^{18}O$, modal abundances of the equilibrium assemblages at the conditions of garnet growth, and isotope fractionation factors among coexisting phases (e.g., Vho et al., 2020). Here, retrogressed matrix assemblages preclude the use of measured bulk rock compositions and bulk $\delta^{18}O$. Instead, a generic altered MORB composition of Staudigel et al. (1996) is used to represent the primary elemental composition of the Oman eclogites. Full details of the modeling approach are in SM 2.

Using the PTloop 1.0 software and the database DBOXYGEN 2.0.3 (Vho et al., 2019, 2020), an original bulk $\delta^{18}O$ of ~14 ‰ is calculated as being in equilibrium with an average garnet core composition of ~12 ‰ at 480–550 °C. In the same temperature range, pure water with $\delta^{18}O$ of 10.5–13 ‰ would be in equilibrium with Oman garnet rim values of 9–10.5 ‰. Consequently, the decline in $\delta^{18}O$ in the rims of Oman garnet is likely due to infiltration of an external fluid with a $\delta^{18}O$ of 10.5–13 ‰ or lower. Whether the difference in rim compositions between samples from the same outcrop is due to differences in the $\delta^{18}O$ of fluid at given

fluid–rock ratios, or to spatially-variable fluid–rock ratios with a single fluid composition is unknown.

Such a fluid could derive from several sources. In Oman, high-temperature serpentine has $\delta^{18}O$ of 4–7 ‰ (Scicchitano et al., 2021). At temperatures of garnet mantle–rim growth (500–550 °C), the 1–2 wt. % fluids released from serpentinites with $\delta^{18}O$ of 5 ‰ is calculated to have a $\delta^{18}O$ of 6.5–6.9 ‰. Alternatively, heavier $\delta^{18}O$ fluids (9–16 ‰) derived from sedimentary sources with bulk $\delta^{18}O$ of 14–26 ‰ (Bebout and Barton, 1989) may have driven the observed decline in $\delta^{18}O$ in the Oman garnet. Lastly, lawsonite, containing 11.5 wt.% H_2O, liberates heavy $\delta^{18}O$ fluid (>14 ‰) during prograde dehydration. Previous work suggested that fluid release associated with lawsonite breakdown may be associated with a fO_2 reduction in the residual assemblage, and a concomitant decline in the andradite component incorporated in garnet (Gerritts et al., 2019).

We explore the above scenarios to investigate fluid–rock ratios experienced by the Oman eclogites. Phase relations and isotope fractionation in altered MORB with an initial $\delta^{18}O$ of 14 ‰ were simulated along a *P–T* path from 1.4 GPa and 375 °C to 2.0 GPa and 550 °C (Fig. 7a). In a closed system, internally-produced H_2O increases to ~14 vol% after lawsonite dehydration, but $\delta^{18}O$ in garnet changes by only ~0.5 ‰ over the modelled path (Fig. 7a, b). External fluid infiltration is also simulated to occur in a single episode at 500 °C. By varying the mass of infiltrating fluid, fluid–rock ratios required to shift the $\delta^{18}O$ composition in growing garnet—from ~12.5 ‰ in the core to 9–10.5 ‰ in the rim—were evaluated.

For serpentinite-derived fluids ($\delta^{18}O$ of ~6.7 ‰), time-integrated infiltration of 6.6×10^4–1.3×10^5 kg of H_2O is required to reduce garnet $\delta^{18}O$ by 2–3.5 ‰, yielding fluid–rock mass ratios of 0.2–0.4 (Fig. 7c). In the case of isotopically-heavier sediment-derived fluids ($\delta^{18}O$ of ~12.5 ‰), greater volumes of fluid are required to buffer the same change in garnet composition: at least 2×10^6 kg of H_2O and fluid–rock mass ratios >6 are required (Fig. 7d). The effect of lawsonite dehydration on garnet $\delta^{18}O$ is negligible (see discussion in SM 2). Given evidence that these isotopic compositions in garnet did not equilibrate at the thin section scale and the assumption that fluids had not equilibrated with isotopically heavier crustal components during transfer, these fluid–rock ratios are likely minimum estimates. The calculated values yield time-integrated fluxes of $1.0–1.65 \times 10^4$ cm^3/cm^2 in the case of serpentinite-derived fluids and $>2.0 \times 10^5$ cm^3/cm^2 for sediment-derived fluids, respectively.

Associated variation in elemental chemistry offers additional constraints: as antigorite-derived fluids are generally enriched in Ca, Cr and LREE–MREE (Spandler et al., 2011, Spandler et al., 2014; Pettke and Bretscher, 2022), and the elemental changes associated with the fluid infiltration boundary in the Oman garnets (Fig. 1 and SM 3) may support infiltration of such isotopically lighter, ultramafic-derived fluids. Fluid rock ratios of 1.65×10^4 cm^3/cm^2 for serpentinite-derived fluids are consistent with threshold values of 10^4 cm^3/cm^2 for open system fluid flow hypothesized by Zack and John (2007), but are an order of magnitude lower than those of Bovay et al. (2021) and Vho et al. (2020b), who suggest that pervasive (porous/grain boundary) flow in *HP–LT* systems can accommodate fluid–rock ratios in excess of 10^4 cm^3/cm^2. The absence of significant oxygen isotope evidence for fluid buffering during the main stage of garnet growth in four of the five subduction systems studied is consistent with proposals that long-distance fluid transfer in subduction may be highly localized/channelized (e.g., Camacho et al., 2005; John et al., 2012; Taetz et al., 2018).

5. Conclusions

This study reveals a complex picture of element and oxygen isotope transfer at high pressure during subduction. Oscillatory elemental zoning in garnet that is present in many rocks from *HP–LT* complexes and which may reflect some fundamental process forms from effective

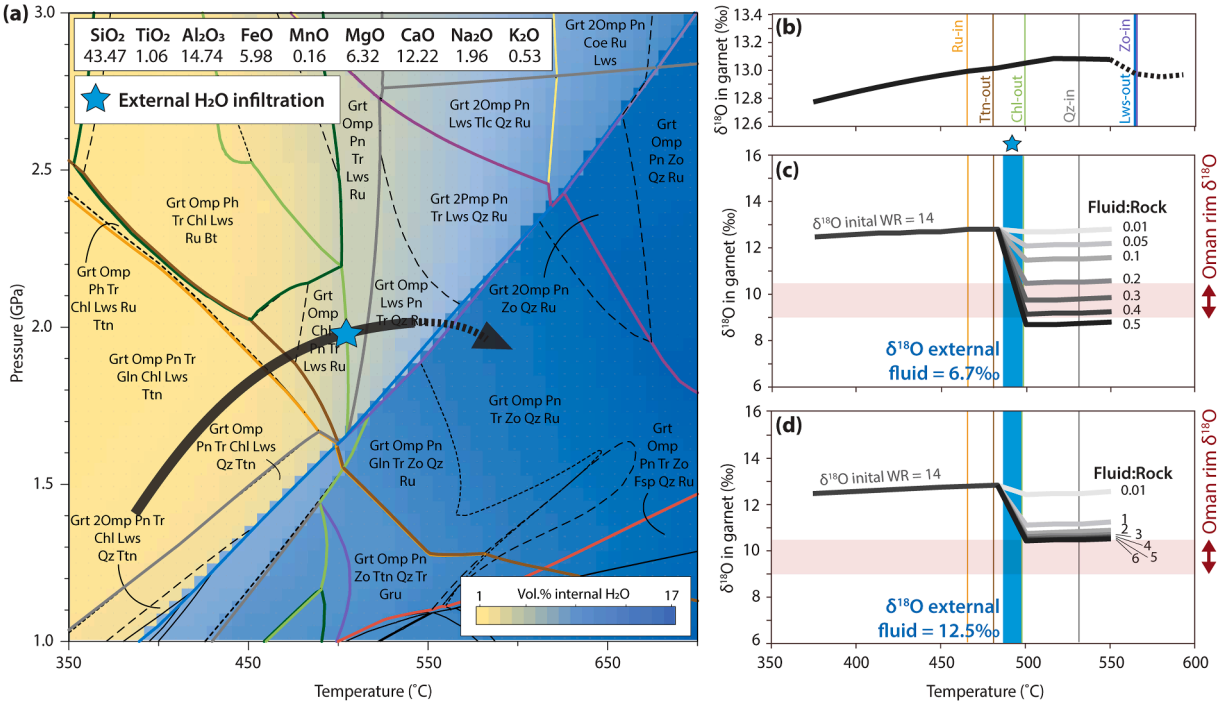

Fig. 7. Results of phase equilibria and fluid–rock interaction modeling. (a) Phase equilibria for average altered metabasalt of Staudigel et al. (1996). Pressure–temperature path and peak metamorphic conditions of Oman eclogite evolution adopted from Warren and Waters (2001) and Searle et al. (1994). Blue star represents position/timing of simulated fluid ingress, short, dashed line shows additional *P–T* evolution required to dehydrate lawsonite. Mineral abbreviations after Whitney and Evans (2010). (b) Modelled $\delta^{18}O$ in garnet v. temperature along the full (including dashed) prograde path in (a), with no external fluid infiltration. (c) Modelled $\delta^{18}O$ in garnet v. temperature along solid line in (b) for infiltration of serpentinite-derived fluid with $\delta^{18}O = 6.7\%$. (d) As in (c) but for sediment-derived fluid with $\delta^{18}O = 12.5\%$.

bulk compositions that are equilibrated at across the centimeter-scale, but cannot be simply linked to external fluid ingress that buffers the composition of the growing garnet. The observed elemental oscillations may record transient episodes of rock-wide equilibration during prograde metamorphism, as has been proposed by Konrad-Schmolke et al. (2023), but must be decoupled from the fluid transfer processes recorded by oxygen isotopes. Alternatively, pulse-like changes in element solubility or efficiency of transport properties of the grain boundaries, decoupled from local pulses of fluid transfer and changes in isotopic composition of garnet, may require consideration.

Combined, the oxygen isotope zoning is suggestive of significant spatiotemporal heterogeneity and episodicity in chemical transfer in subduction. Evidence from the Oman rocks in this study, in addition to studies from other settings (e.g., Gerritts et al., 2019; Russel et al., 2013; Rubatto and Angiboust, 2015; Bovay et al., 2021), indicate that pervasive infiltration of external fluids can effectively buffer the elemental, isotopic and redox state of the effective bulk rock composition during prograde garnet growth. Californian grains are consistent with external fluid infiltration in only the very final stages of garnet growth and incorporation into the mélange, in line with observations in other studies (Errico et al., 2013; Page et al., 2014; Cruz-Uribe et al., 2021). In contrast, garnet growth in other samples studied here occurred in the presence of fluids whose compositions may have been only locally controlled, within closed systems that vary internally to a magnitude of ~2 ‰. Consistent with previous work (e.g., Camacho et al., 2005; Zack and John, 2007; John et al., 2012; Angiboust and Raimondo, 2022), our results suggest that some blocks of subducting mafic crust can maintain low permeability to sub-arc depths, and that the majority of fluid transfer in subduction may be accommodated via spatially discrete, episodic events.

CRediT authorship contribution statement

Freya R. George: Writing – review & editing, Writing – original draft, Visualization, Validation, Software, Resources, Project administration, Methodology, Investigation, Funding acquisition, Formal analysis, Data curation, Conceptualization. **Daniel R. Viete:** Writing – review & editing, Validation, Project administration, Methodology, Investigation, Funding acquisition, Data curation, Conceptualization. **Janaína Ávila:** Writing – review & editing, Formal analysis. **Gareth G. E. Seward:** Writing – review & editing, Formal analysis. **George L. Guice:** Writing – review & editing, Formal analysis. **Mark B. Allen:** Writing – review & editing, Resources, Funding acquisition. **Michael J. Harrower:** Writing – review & editing, Resources, Funding acquisition.

Declaration of competing interest

The authors declare that they have no known competing financial interests or personal relationships that could have appeared to influence the work reported in this paper.

Data availability

Data will be made available on request.

Acknowledgments

We thank Zeb Page and an anonymous reviewer for their very thorough and thoughtful reviews, which significantly improved the presentation of this research. Rosemary Hickey-Vargas is thanked for editorial handling and suggestions that also improved the quality of this work. The Smithsonian Institution's National Museum of Natural History is thanked for facilitating loans of samples from the Dominican Republic. Sampling in Greece, Oman and Venezuela was enabled by funding and/or field support from B.R. Hacker, E.M. Scott, H.A. Viete, Fulbright Australia and the Geological Society of London. G. Poirer and D. Dierkrup provided EPMA assistance at the University of Ottawa. FRG acknowledges financial support from the US–UK Fulbright Commission and Lloyd's of London in addition to a Blaustein Fellowship in the Department of Earth & Planetary Sciences, JHU. Microprobe work at the University of Ottawa and UCSB and SIMS work at the Australian National University was funded by JHU, UCSB and funds attached to the Blaustein Fellowship to FRG. Trace element raster mapping by LA–ICP–MS was supported by an NSF-EAR/IF grant (NSF-1831766) to DRV and MJH.

Supplementary materials

Supplementary material associated with this article can be found, in the online version, at doi:10.1016/j.epsl.2024.118634.

References

Angiboust, S., Raimondo, T., 2022. Permeability of subducted oceanic crust revealed by eclogite-facies vugs. Geology 50 (8), 964–968.
Angiboust, S., Pettke, T., De Hoog, J.C., Caron, B., Oncken, O., 2014. Channelized fluid flow and eclogite-facies metasomatism along the subduction shear zone. J. Petrol. 55 (5), 883–916.
Anczkiewicz, R., Platt, J.P., Thirlwall, M.F., Wakabayashi, J., 2004. Franciscan subduction off to a slow start: evidence from high-precision Lu–Hf garnet ages on high grade-blocks. Earth Planet. Sci. Lett. 225 (1–2), 147–161.
Baumgartner, L.P., Valley, J.W., 2001. Stable isotope transport and contact metamorphic fluid flow. Rev. Mineral. Geochem. 43 (1), 415–467.
Bebout, G.E., Barton, M.D., 1989. Fluid flow and metasomatism in a subduction zone hydrothermal system: Catalina Schist terrane, California. Geology 17 (11), 976–980.
Blanco-Quintero, Y.R.-A., García-Casco, A., Kroner, A., Mertz, D.F., Lázaro, C., Blanco-Moreno, J., 2010b. Doctoral Thesis. In: Blanco-Quintero, I.F. (Ed.), pp. 59–91.
Blanco-Quintero, A.G.-C., Gerya, T.V., 2011. Tectonic blocks in serpentinite mélange (eastern Cuba) reveal large-scale convective flow of the subduction channel. Geology 39 (1), 79–82.
Bovay, T., Rubatto, D., Lanari, P., 2021. Pervasive fluid-rock interaction in subducted oceanic crust revealed by oxygen isotope zoning in garnet. Contrib. Mineral. Petrol. 176 (7), 1–22.
Camacho, J.K.L., Hensen, B.J., Braun, J., 2005. Short-lived orogenic cycles and the eclogitization of cold crust by spasmodic hot fluids. Nature 435 (7046), 1191–1196.
Carlson, W.D., Hixon, J.D., Garber, J.M., Bodnar, R.J., 2015. Controls on metamorphic equilibration: the importance of intergranular solubilities mediated by fluid composition. J. Metamorph. Geol. 33 (2), 123–146.
Cisneros, M., Behr, W.M., Platt, J.P., Anczkiewicz, R., 2022. Quartz-in-garnet barometry constraints on formation pressures of eclogites from the Franciscan Complex, California. Contrib. Mineral. Petrol. 177 (1), 12.
Codillo, E.A., Roux, V.L., Marschall, H.R., 2018. Arc-like magmas generated by mélange-peridotite interaction in the mantle wedge. Nat. Commun. 9 (1), 1–11.
Connolly, J.A., Podladchikov, Y.Y., 2004. Fluid flow in compressive tectonic settings: implications for midcrustal seismic reflectors and downward fluid migration. J. Geophys. Res. 109 (B4).
Cruz-Uribe, F.Z.P., Lozier, E., Feineman, M.D., Zack, T., Mertz-Kraus, R., Jacob, D.E., Kitajima, K., 2021. Trace element and isotopic zoning of garnetite veins in amphibolitized eclogite, Franciscan Complex, California, USA. Contrib. Mineral. Petrol. 176 (5), 1–19.
Dudley, P., 1969. Electron microprobe analyses of garnet in glaucophane schists and associated eclogites. Am. Mineral. 54 (7–8), 1139–1150.
Elkhoury, J.E., Brodsky, E.E., Agnew, D.C., 2006. Seismic waves increase permeability. Nature 441 (7097), 1135–1138.
Errico, J.C., Barnes, J.D., Strickland, A., Valley, J.W., 2013. Oxygen isotope zoning in garnets from Franciscan eclogite blocks: evidence for rock–buffered fluid interaction in the mantle wedge. Contrib. Mineral. Petrol. 166, 1161–1176.
Ferry, J.M., Kitajima, K., Strickland, A., Valley, J.W., 2014. Ion microprobe survey of the grain-scale oxygen isotope geochemistry of minerals in metamorphic rocks. Geochim. Cosmochim. Acta 144, 403–433.
Garber, J.M., Rioux, M., Searle, M.P., Kylander-Clark, A.R., Hacker, B.R., Vervoort, J.D., Smye, A.J., 2021. Dating continental subduction beneath the Samail Ophiolite: garnet, zircon, and rutile petrochronology of the As Sifah eclogites, NE Oman. J. Geophys. Res. 126 (12), e2021JB022715.
García-Casco, R.L.T.-R., Millán, G., Monié, P., Schneider, J., 2002. Oscillatory zoning in eclogitic garnet and amphibole, Northern Serpentinite Melange, Cuba: a record of tectonic instability during subduction? J. Metamorph. Geol. 20 (6), 581–598.
George, F.R., Gaidies, F., 2017. Characterisation of a garnet population from the Sikkim Himalaya: insights into the rates and mechanisms of porphyroblast crystallisation. Contrib. Mineral. Petrol. 172 (7), 57.
George, F.R., Gaidies, F., Boucher, F.B., 2018. Population-wide garnet growth zoning revealed by LA-ICP-MS mapping: implications for trace element equilibration and syn-kinematic deformation during crystallisation. Contrib. Mineral. Petrol. 173, 1–22.
George, F.R., Viete, D.R., Ávila, J., Seward, G.G., 2021. Decoupled oscillatory and O-isotope zonation in high pressure low temperature garnet: records of heterogeneous

fluid transfer processes. In: EGU General Assembly Conference Abstracts, pp. EGU21–E3061.
Gerrits, E.C.I., Dragovic, B., Starr, P.G., Baxter, E.F., Burton, K.W., 2019. Release of oxidizing fluids in subduction zones recorded by iron isotope zonation in garnet. Nat. Geosci. 12 (12), 1029–1033.
Hickmott, D.D., Sorensen, S.S., Rogers, P.S.Z., 1992. Metasomatism in a subduction complex: constraints from microanalysis of trace elements in minerals from garnet amphibolite from the Catalina Schist. Geology 20 (4), 347–350.
Higashino, F., Rubatto, D., Kawakami, T., Bouvier, A.S., Baumgartner, L.P., 2019. Oxygen isotope speedometry in granulite facies garnet recording fluid/melt–rock interaction (Sør Rondane Mountains, East Antarctica). J. Metamorph. Geol. 37 (7), 1037–1048.
Holness, M.B., 1993. Temperature and pressure dependence of quartz-aqueous fluid dihedral angles: the control of adsorbed H_2O on the permeability of quartzites. Earth Planet. Sci. Lett. 117 (3–4), 363–377.
Hoover, W.F., Penniston-Dorland, S., Baumgartner, L., Bouvier, A.S., Dragovic, B., Locatelli, M., Angiboust, S., Agard, P., 2022. Episodic fluid flow in an eclogite-facies shear zone: Insights from Li isotope zoning in garnet. Geology 50 (6), 746–750.
Hyppolito, T., Cambeses, A., Angiboust, S., Raimondo, T., García-Casco, A., Juliani, C., 2019. Rehydration of eclogites and garnet-replacement processes during exhumation in the amphibolite facies. Geol. Soc. London, Special Pub. 478 (1), 217–239.
Jamtveit, B., Ragnarsdottir, K.V., Wood, B.J., 1995. On the origin of zoned grossular-andradite garnets in hydrothermal systems. Eur. J. Mineral. 7 (6), 1399–1410.
Jedlicka, R., Faryad, S.W., Hauzenberger, C., 2015. Prograde metamorphic history of UHP granulites from the Moldanubian Zone (Bohemian Massif) revealed by major element and Y+ REE zoning in garnets. J. Petrol. 56 (10), 2069–2088.
John, T., Gussone, N., Podladchikov, Y.Y., Bebout, G.E., Dohmen, R., Halama, R., Magna, T., Seitz, H.M., 2012. Volcanic arcs fed by rapid pulsed fluid flow through subducting slabs. Nat. Geosci. 5 (7), 489–492.
Kabir, M.F., Takasu, A., 2010. Evidence for multiple burial–partial exhumation cycles from the Onodani eclogites in the Sambagawa metamorphic belt, central Shikoku, Japan. J. Metamorph. Geol. 28 (8), 873–893.
Kessel, R., Pettke, T., Fumagalli, P., 2015. Melting of metasomatized peridotite at 4–6 GPa and up to 1200 °C: an experimental approach. Contrib. Mineral. Petrol. 169 (4), 37.
Kogiso, T., Tatsumi, Y., Nakano, S., 1997. Trace element transport during dehydration processes in the subducted oceanic crust: 1. Experiments and implications for the origin of ocean island basalts. Earth Planet. Sci. Lett. 148 (1–2), 193–205.
Kohn, M.J., Valley, J.W., Elsenheimer, D., Spicuzza, M.J., 1993. O isotope zoning in garnet and staurolite: evidence for closed-system mineral growth during regional metamorphism. Am. Mineral. 78 (9–10), 988–1001.
Konrad-Schmolke, M., Zack, T., O'Brien, P.J., Jacob, D.E., 2008. Combined thermodynamic and rare earth element modelling of garnet growth during subduction: examples from ultrahigh-pressure eclogite of the Western Gneiss Region, Norway. Earth Planet. Sci. Lett. 272 (1–2), 488–498.
Konrad-Schmolke, M., Halama, R., Chew, D., Heuzé, C., De Hoog, J., Ditterova, H., 2023. Discrimination of thermodynamic and kinetic contributions to the heavy rare earth element patterns in metamorphic garnet. J. Metamorph. Geol. 41 (4), 465–490.
Kulhánek, J., Faryad, S.W., 2023. Compositional changes in garnet: trace element transfer during eclogite-facies metamorphism. Contrib. Mineral. Petrol. 178 (10), 68.
Lagos, M., Scherer, E.E., Tomaschek, F., Münker, C., Keiter, M., Berndt, J., Ballhaus, C., 2007. High precision Lu–Hf geochronology of Eocene eclogite-facies rocks from Syros, Cyclades, Greece. Chem. Geol. 243 (1–2), 16–35.
Li, J.L., Klemd, R., Gao, J., John, T., 2016. Poly-cyclic metamorphic evolution of eclogite: evidence for multistage burial–exhumation cycling in a subduction channel. J. Petrol. 57 (1), 119–146.
Martin, L.A., Rubatto, D., Crépisson, C., Hermann, J., Putlitz, B., Vitale-Brovarone, A., 2014. Garnet oxygen analysis by SHRIMP-SI: matrix corrections and application to high-pressure metasomatic rocks from Alpine Corsica. Chem. Geol. 374, 25–36.
Mibe, K., Yoshino, T., Ono, S., Yasuda, A., Fujii, T., 2003. Connectivity of aqueous fluid in eclogite and its implications for fluid migration in the Earth's interior. J. Geophys. Res. 108 (B6).
Moore, S.J., Carlson, W.D., Hesse, M.A., 2013. Origins of yttrium and rare earth element distributions in metamorphic garnet. J. Metamorph. Geol. 31 (6), 663–689.
Page, F.Z., Essene, E.J., Mukasa, S.B., Valley, J.W., 2014. A garnet–zircon oxygen isotope record of subduction and exhumation fluids from the Franciscan Complex, California. J. Petrol. 55 (1), 103–131.
Page, F.Z., Cameron, E.M., M.Flood, C., Dobbins, J.W., Spicuzza, M.J., Kitajima, K., Valley, J.W., 2019. Extreme oxygen isotope zoning in garnet and zircon from a metachert block in mélange reveals metasomatism at the peak of subduction metamorphism. Geology 47 (7), 655–658.
Penniston-Dorland, S.C., Baumgartner, L.P., Dragovic, B., Bouvier, A.S., 2020. Li isotope zoning in garnet from Franciscan eclogite and amphibolite: the role of subduction-related fluids. Geochim. Cosmochim. Acta 286, 198–213.
Pettke, T., Bretscher, A., 2022. Fluid-mediated element cycling in subducted oceanic lithosphere: The orogenic serpentinite perspective. Earth Sci. Revs. 225, 103896.
Piccoli, F., Ague, J.J., Chu, X., Tian, M., Vitale Brovarone, A., 2021. Field-based evidence for intra-slab high-permeability channel formation at eclogite-facies conditions during subduction. Geochem., Geophys., Geosyst. 22 (3), e2020GC009520.
Plümper, O., John, T., Podladchikov, Y.Y., Vrijmoed, J.C., Scambelluri, M., 2017. Fluid escape from subduction zones controlled by channel-forming reactive porosity. Nat. Geosci. 10 (2), 150–156.
Putlitz, B., Matthews, A., Valley, J.W., 2000. Oxygen and hydrogen isotope study of high-pressure metagabbros and metabasalts (Cyclades, Greece): implications for the subduction of oceanic crust. Contrib. Mineral. Petrol. 138, 114–126.
Rubatto, D., Angiboust, S., 2015. Oxygen isotope record of oceanic and high-pressure metasomatism: a P–T–time–fluid path for the Monviso eclogites (Italy). Contrib. Mineral. Petrol. 170 (5), 1–16.
Rubatto, D., Burger, M., Lanari, P., Hattendorf, B., Schwarz, G., Neff, C., Keresztes Schmidt, P., Hermann, J., Vho, A., Günther, D., 2020. Identification of growth mechanisms in metamorphic garnet by high-resolution trace element mapping with LA-ICP-TOFMS. Contrib. Mineral. Petrol. 175 (7), 61.
Russell, K., Kitajima, K., Strickland, A., Medaris, L.G., Schulze, D.J., Valley, J.W., 2013. Eclogite-facies fluid infiltration: constraints from $\delta^{18}O$ zoning in garnet. Contrib. Mineral. Petrol. 165 (1), 103–116.
Pyle, J.M., Spear, F.S., 1999. Yttrium zoning in garnet: coupling of major and accessory phases during metamorphic reactions. Geol. Materia. Res. 1 (6), 1–49.
Schmidt, M.W., Poli, S., 1998. Experimentally based water budgets for dehydrating slabs and consequences for arc magma generation. Earth Planet. Sci. Lett. 163 (1–4), 361–379.
Schumacher, R., Rötzler, K., Maresch, W.V., 1999. Subtle oscillatory zoning in garnet from regional metamorphic phyllites and mica schists, western Erzgebirge, Germany. Can. Mineral. 37 (2), 381–403.
Scicchitano, M.R., Spicuzza, M.J., Ellison, E.T., Tuschel, D., Templeton, A.S., Valley, J. W., 2021. Situ oxygen isotope determination in serpentine minerals by SIMS: addressing matrix effects and providing new insights on serpentinisation at hole BA1B (Samail ophiolite, Oman). Geostand. Geoanal. Res. 45 (1), 161–187.
Smye, J., Warren, C.J., Bickle, M.J., 2013. The signature of devolatisation: extraneous ^{40}Ar systematics in high-pressure metamorphic rocks. Geochim. Cosmochim. Acta 113, 94–112.
Spandler, C., Pettke, T., Hermann, J., 2014. Experimental study of trace element release during ultrahigh-pressure serpentinite dehydration. Earth Planet. Sci. Lett. 391, 296–306.
Spandler, T.P., Rubatto, D., 2011. Internal and external fluid sources for eclogite-facies veins in the Monviso meta-ophiolite, Western Alps: implications for fluid flow in subduction zones. J. Petrol. 52 (6), 1207–1236.
Staudigel, H., Plank, T., White, T.B., Schmincke, H.U., 1996. Geochemical fluxes during seafloor alteration of the basaltic upper oceanic crust: DSDP Sites 417 and 418. Subduction 96, 19–38.
Stowell, H.H., Menard, T., Ridgway, C.K., 1996. Ca-metasomatism and chemical zonation of garnet in contact-metamorphic aureoles, Juneau Gold Belt, southeastern Alaska. Can. Mineral. 34 (6), 1195–1209.
Taetz, S., John, T., Bröcker, M., Spandler, C., Stracke, A., 2018. Fast intraslab fluid-flow events linked to pulses of high pore fluid pressure at the subducted plate interface. Earth Planet. Sci. Lett. 482, 33–43.
Tan, Z., Agard, P., Gao, J., Hong, T., Wan, B., 2020. Concordant pulse in Mn, Y and HREEs concentrations during UHP eclogitic garnet growth: transient rock dynamics along a cold subduction plate interface. Earth Planet. Sci. Lett. 530, 115908.
Tajčmanová, L., Podladchikov, Y., Powell, R., Moulas, E., Vrijmoed, J.C., Connolly, J.A. D., 2014. Grain-scale pressure variations and chemical equilibrium in high-grade metamorphic rocks. J. Metamorph. Geol. 32 (2), 195–207.
Tamblyn, R., Hand, M., Kelsey, D., Anczkiewicz, R., Och, D., 2020. Subduction and accumulation of lawsonite eclogite and garnet blueschist in eastern Australia. J. Metamorph. Geol. 38 (2), 157–182.
Tsay, Z.Z., Ulmer, P., Sanchez-Valle, C., 2017. Mobility of major and trace elements in the eclogite-fluid system and element fluxes upon slab dehydration. Geochim. Cosmochim. Acta 198, 70–91.
Tual, L., Smit, M.A., Cutts, J., Kooijman, E., Kielman-Schmitt, M., Majka, J., Foulds, I., 2022. Rapid, paced metamorphism of blueschists (Syros, Greece) from laser-based zoned Lu-Hf garnet chronology and LA-ICPMS trace element mapping. Chem. Geol. 607, 121003.
Walters, J.B., Cruz-Uribe, A.M., Song, W.J., Gerbi, C., Biela, K., 2022. Strengths and limitations of in situ U–Pb titanite petrochronology in polymetamorphic rocks: An example from western Maine, USA. J. Metamorph. Geol. 40 (6), 1043–1066.
Warren, C.J., Sherlock, S.C., Kelley, S.P., 2011. Interpreting high-pressure phengite 40 Ar/39 Ar laserprobe ages: an example from Saih Hatat, NE Oman. Contrib. Mineral. Petrol. 161 (6), 991–1009.
Vho, P.L., Rubatto, D., 2019. An internally-consistent database for oxygen isotope fractionation between minerals. J. Petrol. 60 (11), 2101–2129.
Vho, P.L., Rubatto, D., Hermann, J., 2020. Tracing fluid transfers in subduction zones: an integrated thermodynamic and $\delta^{18}O$ fractionation modelling approach. Solid Earth 11 (2), 307–328.
Vielzeuf, D., Veschambre, M., Brunet, F., 2005. Oxygen isotope heterogeneities and diffusion profile in composite metamorphic-magmatic garnets from the Pyrenees. Am. Min. 90 (2–3), 463–472.
Viete, D.R., Kylander-Clark, A.R., Hacker, B.R., 2015. Single-shot laser ablation split stream (SS-LASS) petrochronology deciphers multiple, short-duration metamorphic events. Chem. Geol. 415, 70–86.
Viete, D.R., Hacker, B.R., Allen, M.B., Seward, G.G., Tobin, M.J., Kelley, C.S., Cinque, G., Duckworth, A.R., 2018. Metamorphic records of multiple seismic cycles during subduction. Sci. Adv. 4 (3), eaaq0234.
Yardley, W.D., Rochelle, C.A., Barnicoat, A.C., Lloyd, G.E., 1991. Oscillatory zoning in metamorphic minerals: an indicator of infiltration metasomatism. Mineral. Mag. 55 (380), 357–365.
Zack, T., John, T., 2007. An evaluation of reactive fluid flow and trace element mobility in subducting slabs. Chem. Geol. 239 (3–4), 199–216.